Electronic Supplementary Information

Antireflective Structures on Highly Flexible and Large Area Elastomer Membrane for Tunable Liquid-filled Endoscopic Lens

Sang-In Bae, Youngseop Lee, Yeong-Hyeon Seo, and Ki-Hun Jeong*

Department of Bio and Brain Engineering, KAIST Institute for Health Science and Technology, Korea Advanced Institute of Science and Technology (KAIST), 291 Daehak-ro, Yuseong-gu, Daejeon 34141, Republic of Korea

*Corresponding author. kjeong@kaist.ac.kr (Ki-Hun Jeong)

Supplementary Experimental Section

Nanofabrication of the Glass Nanoholes Template: First and second silver thin film were deposited by using thermal evaporation in Volmer-Weber mode and are annealed on different temperature (450°C in an oven for 40 mins and 380°C on a hot plate for 1 hour). The glass substrate was anisotropically etched by using RIE with CHF_3 of 45 standard cubic centimeters per minute (sccm), CF_4 of 15 sccm and Ar of 150 sccm, a pressure of 200 mTorr, and radio frequency power of 300 W. Etching time controlled the desirable etch depth of GNHs. Residual nano-satellites less than 15 nm in diameter that hinder PDMS replication were generated after RIE. In addition, the original FF after RIE was insufficient compared with the optimal FF of 0.5. Therefore, short-time of isotropic wet etching using buffered oxide etch (6:1 BOE) solution removed nano-satellites and widened the hole size before AgNHs removal (Supporting information *Figure S2*). The residual AgNHs mask was fully removed in silver etchant composed of iodine and potassium iodine solution (etchant TFA, *Transene Company, Inc.*).

Focal Length Measurement: The focal length tunability was measured by using an optical alignment composed of a projection target, a 533 nm wavelength laser, and the lens. The focal length change was observed by moving the projection target using an xyz positioner. A silicon microtube with 0.5 mm in diameter delivered an optical liquid, 6:4 diluted ethylene glycol with deionized water (DI), to a single pressure channel of the lens. A pressure regulator (PV 830 Pneumatic Picopump, *World Precision Instruments, Inc.)* applied pneumatic pressure into the lens channel at 14 different pressure (Figure 3a). From the calculation, the elastic modulus of PDMS membrane was carried out to 6 MPa. The measured values from AR-TL and TL were well matched with the theoretical values at the same applied pressure.

Transmittance Measurement in Flat and Curved Membrane: Transmittance on flat and curved surface were measured using different optical components depending on the direction of light emitting through the surface. Transmittance on flat surface was measured by using a spectrometer (SP-2300i, *Priceton instruments*) with a collimated white-light LED source. The incident light passed straight through the flat surface, and the transmitted light from the surface was analyzed by a spectrometer after passing a 10× objective lens. On the other hand, transmittance on curved surface was measured by using an integrating sphere and a fiber-coupled spectrometer (SM642, *Spectral Products*) coupled with a single LED source. The incident light passing through the curved surface were refracted all around the integrating sphere, and all the transmitted light were collected to the fiber-coupled spectrometer. Transmittance depending on the different lens curvature were measured at four different pressure (14 *kPa*, 21 *kPa*, 28 *kPa*, and 35 *kPa*), which corresponding ROC are 2.3 mm, 2.0 mm, 1.8 mm, and 1.6 mm, respectively.

Section 1. Detailed comparison of silver nanostructures generated from a template-confined solid-state dewetting and a single solid-state dewetting

Fabrication of large-area silver nanostructures is the most important procedure because the nanostructures are a metal mask for PDMS nanopillars replication. The nanostructures as a metal mask should be fabricated in a shape of nanoholes with an optimal period and a fill factor (FF) to satisfy both antireflection over the whole visible region and PDMS replication. A single solid-state dewetting (single dewetting) of a silver thin film easily generates large-area silver nanostructures from nanoislands to nanoholes depending on the deposition thickness and the annealing temperature. However, a single dewetting of a silver film hardly forms the desired silver nanoholes (AgNHs) because these nanostructures are easily disconnected according to the surface energy at the metal - substrate interface. Alternatively, a template-confined repeated solid-state dewetting (template dewetting) of a silver thin film can generate desired AgNHs. A single dewetting of the silver thin film generates Ag nanoislands (AgNIs), which acts as the nanotemplate. A 2nd silver thin film deposited on the nanotemplate connects the AgNIs through thermal annealing and generates the AgNHs by controlling the silver film thickness and the annealing temperature.

Table S1. Comparison of large-area silver nanostructures generated from a template dewetting and a single dewetting. The optimal AgNHs were generated by a template dewetting of a 15 nm and a 20 nm thick silver thin films.

	Template-confined repeated solid-state dewetting		**Single solid-state dewetting**	
Metal mask pattern	Nanoislands	Nanoholes	Nanoholes	Nanoholes
Ag film thickness	15 nm	1st 15 nm / 2nd 20 nm	35 nm	16 nm
Annealing temperature	450 ˚C (Oven)	450 ˚C (Oven) / 380 ˚C (Hot plate)	380 ˚C (Hot plate)	150 ˚C (Hot plate)

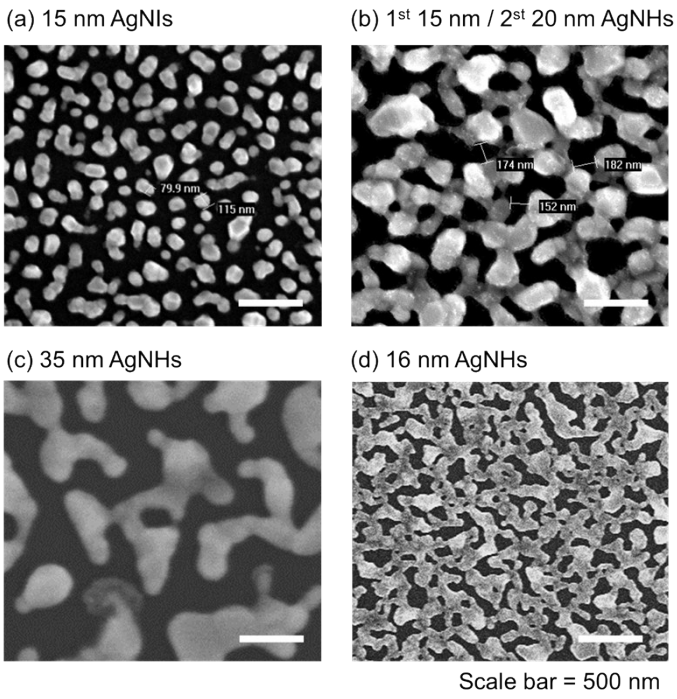

Fig. S1 SEM images of large-area silver nanostructures generated from a template-confined repeated solid-state dewetting (template dewetting) and a single solid-state dewetting (single dewetting). (a) Thermal annealing of a 15 nm thick silver film in an oven at 450 °C for 40 mins generates Ag nanoislands, which act as a pre-determined nanotemplate for the next step annealing. (b) A 20 nm thick silver film was deposited on the nanotemplate of Ag nanoislands and annealed on a hot plate at 380 °C for 60 mins. Ag nanoholes (AgNHs) were generated from the processes, which have the optimal period and the fill factor (FF) satisfying antireflection and PDMS replication. (c) Unlike template dewetting, nanostructures generated from a single dewetting of a silver film with a thickness of 35 nm has larger period than antireflection criteria. (d) A single dewetting of silver film with a thickness of 16 nm has tiny nanoholes, not suitable to replicate the PDMS nanopillars.

Section 2. SEM and AFM images of an antireflective membrane and geometrical characterization of AR-TL

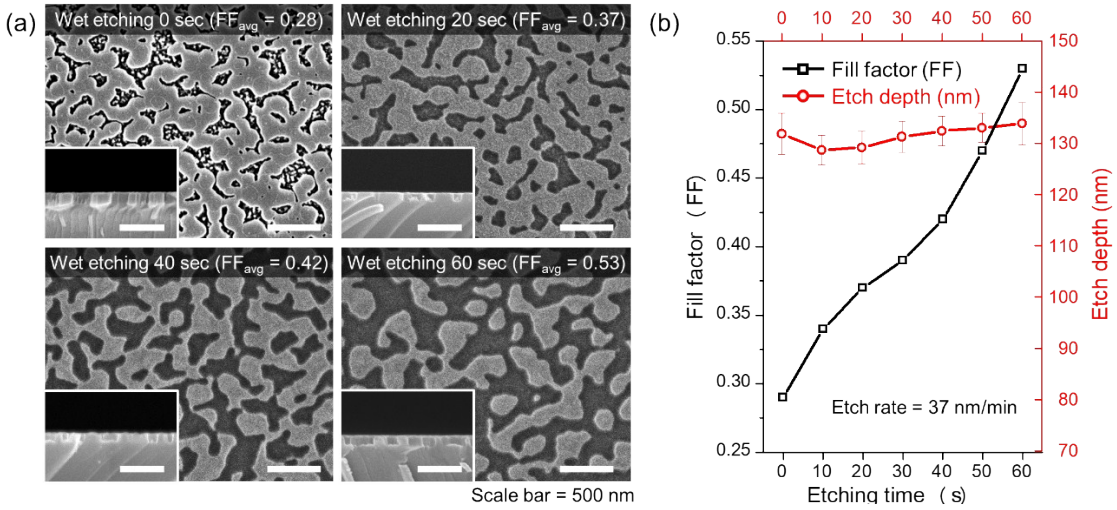

Fig. S2 The FF and the etch depth of GNHs depending on the etching time in buffered oxide etchant (BOE, 6:1 diluted). (a) Top and cross-sectional SEM images of GNHs with different etching times of 0, 20, 40, and 60 sec, (b) The FFs and the etch depths depending on the etching time. Wet etching in BOE removes not only nano-satellites between the nanoholes but also enlarges the nanohole diameter. The vertical depth moderately maintains during the wet etching due to the porous nature of silver thin film mask. In contrast, the FF linearly increases with the etching time. In this experiment, the wet etching was performed for 50 sec to obtain the FF of 0.5**.**

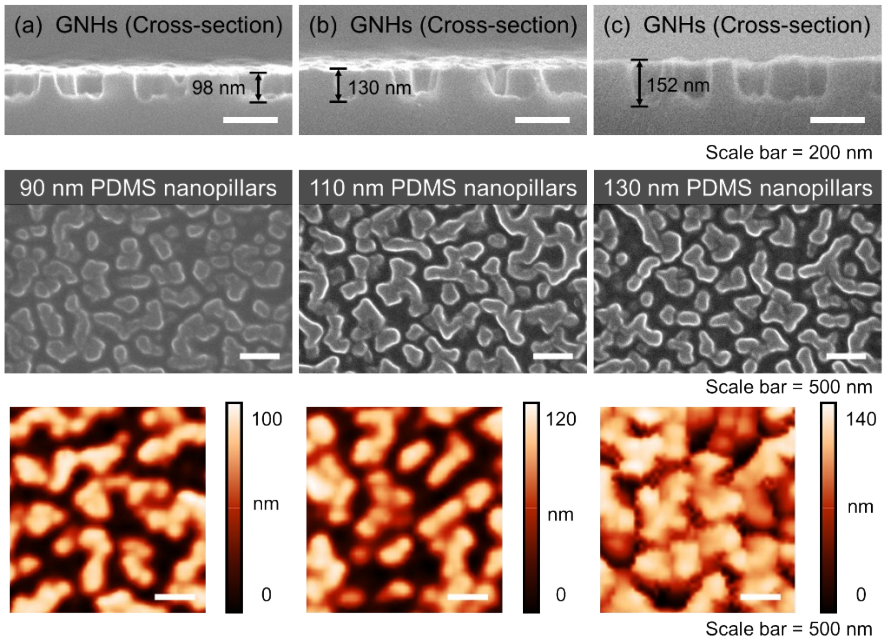

Fig. S3 SEM and AFM images of GNHs and PDMS replica with different nanopillars of (a) 90 nm, (b) 110 nm, and (c) 130 nm in height. The depth of GNHs was controlled approximately using the etching time and the measured etch rate during the reactive ion etching. Besides, the depth was also controlled slightly higher than the calculated value to compensate for both the shrinkage and the replication fidelity for the nanoholes during the PDMS curing. PDMS nanopillars have an averaged period of 246 nm and a FF of 0.49. The AFM images also demonstrated that the heights of the nanopillars were successfully transferred from the GNHs template.

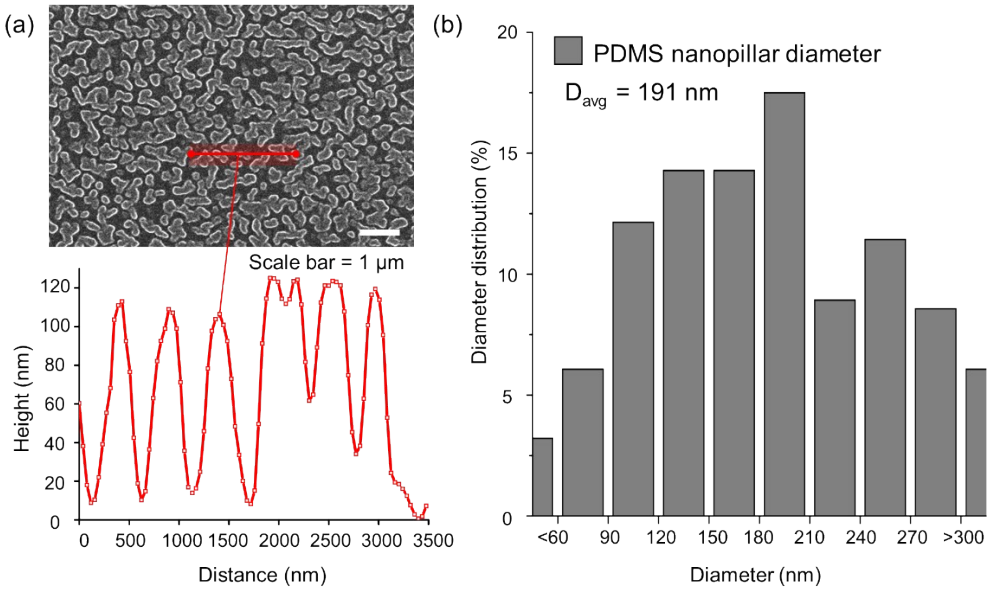

Fig. S4 Geometrical parameters of PDMS nanopillars extracted from the SEM and AFM images. (a) A cross-sectional distribution of 110 nm nanopillars in height, based on the AFM data, clearly indicates that GNHs template successfully transferred PDMS nanopillars considering replication fidelity and shrinkage during PDMS curing. (b) A diameter distribution of the nanopillars extracted by using *Image J* ® from the SEM top view image. The average diameter of the nanopillar is 191 nm and the diameter distribution of the nanopillars is largest in the range of about 180 nm to 210 nm in diameter. The PDMS nanopillars exhibit broadband antireflection over the full visible region owing to the nanopillar size distribution of the acceptable FF and the nanopillar size (based on Figure. 1(c))

Section 3. Detailed device fabrication process

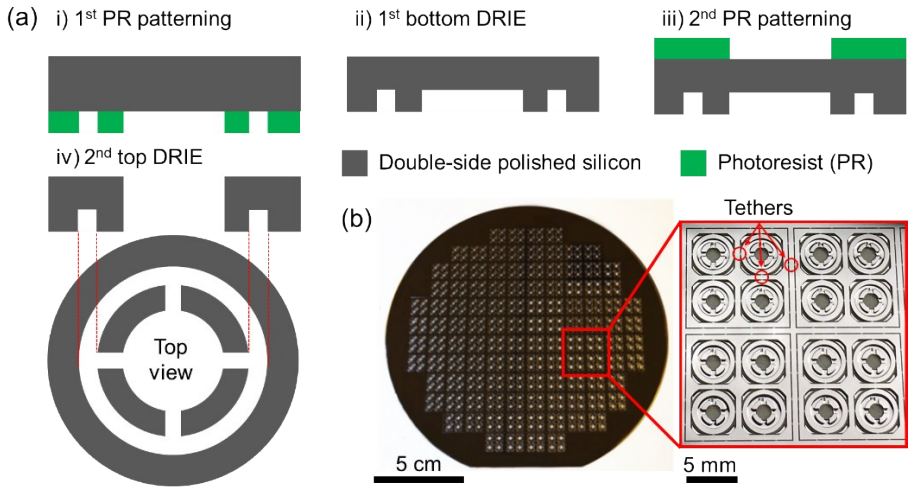

Fig. S5 Microfabrication procedure of micromachined silicon lens mounts with quadrant microchannels. A double-side polished 6-in silicon wafer was photolithographically defined by top and bottom Cr masks. The silicon wafer was etched on both the top and the bottom sides by using deep reactive ion etching (DRIE), which results in the lens mount with outer diameter of 4.0 mm and aperture diameter of 1.5 mm.

Section 4. Numerical analysis of the PDMS nanopillars geometry

1. Forward scattering of PDMS nanopillars depending on the nanopillar period

Geometry of PDMS nanopillars determines whether the nanopillars suppress undesirable specular reflection or the nanopillars scatter and reflect the incident light. A haze factor, i.e., a measure of the degree of scattering in the direction of the incident light by a scatterer or diffuser, is necessary for the structures employing scatterers such as metallic nanoparticles or extraordinary optical transmittance (EOT) structures *(Preston, Colin, et al. "Optical haze of transparent and conductive silver nanowire films." Nano Research 6.7 (2013): 461-468.)*. Therefore, it is possible to verify relatively low transmittance at shorter wavelengths along the nanopillar period by measuring the haze factor.

The degree of scattering of PDMS nanopillars is numerically calculated by using a finite difference time domain (FDTD, Lumerical) method based on Maxwell's equation. The haze factor is defined as a ratio of forward scattered light and a sum of forward non-scattered and scattered light, and a total-field scattered-field (TFSF) source is used to separate a forward scattered light from the sum of forward light (**Fig. S6**). Haze factors of the visible range for the different nanopillar size (150 nm, 250 nm, and 350 nm in period) with a constant height and FF prove that the nanopillars with a period of 250 nm or more can cause forward scattering at shorter wavelengths. Also, the degree of scattering increases exponentially with

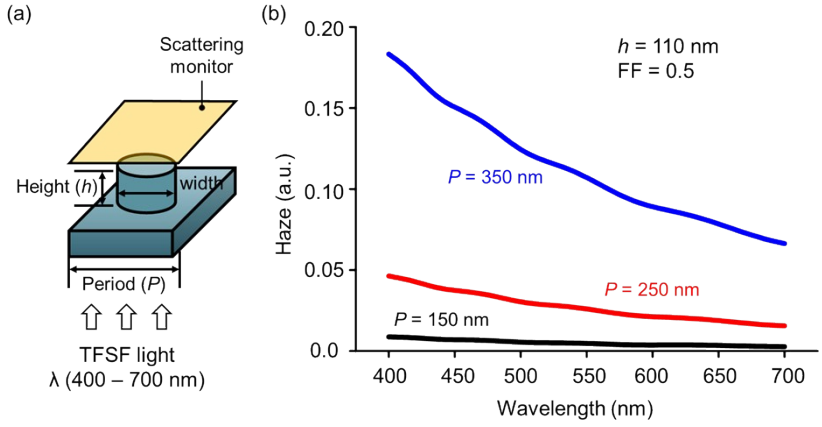

increasing period.

Fig. S6 (a) A schematic illustration of numerical analysis for the haze of PDMS nanopillar. (b) The haze factor of PDMS nanopillars in the visible region of 400 – 700 nm according to the different nanopillar period (150 nm, 250 nm, and 350 nm). The nanopillar height and the fill factor are constant (110 nm in height and 0.5 in fill factor).

2. PDMS nanopillars geometry during membrane deformation

Transmittance enhancement through a curved surface of AR-TL showed that the deformed PDMS nanopillars still satisfied antireflection despite of the membrane deformation. Geometrical parameters of PDMS nanopillars changes during a thin PDMS membrane deformation. PDMS nanopillars shrink or extend their size at the different membrane position, which result in the variation of light transmittance. The geometrical changes depending on the applied strain are analyzed by using the finite element analysis (FEA, COMSOL Multiphysics®) considering an elastic modulus and Poisson's ratio (ν = 0.49) of PDMS (**Table S2**). Variation in transmittance during deformation of the PDMS membrane with nanopillars are numerically calculated by using the FDTD method based on the geometrical parameters calculated from the **Table S2**. Geometrical parameters at x_1 and x_2 positions increase slightly but still satisfy the antireflection condition. Also, the top width at both points is smaller than the those of bottom width, and thus those nanopillars have a trapezoid shape, which enables gradual matching of the effective refractive index. At x_3 position, in contrast, the height, the period, and the top width of the nanopillars are not changed, but the bottom width of the nanopillars are shrank due to the compressive stress at the bottom. An inverse trapezoid shape at x_3 position induces an inverse profile of an effective refractive index, which results in slight transmittance variation of 0.6 %. The geometry of the deformed nanopillars was slightly changed, and the FF was maintained around ~0.5, which are within the antireflection criteria.

Table S2. Geometrical changes of PDMS nanopillars during deformation of a thin PDMS membrane. The nanopillars of 110 nm in height changes to 120 nm, 110 nm, and 110 nm, and the FF varies with 0.45, 0.48, and 0.48 at each of the x_1, x_2, and x_3 positions, respectively.

Nanopillar dimension (nm)	**Flat (0 mm)**	**Maximum deformation (0.23 mm, ΔP = 42 *kPa*)**		
		x_1	**x_2**	**x_3**
Height	110 nm	120 nm	110 nm	110 nm
Period	246 nm	261 nm	270 nm	246 nm
Top width	193 nm	192 nm	209 nm	193 nm
Bottom width		201 nm	214 nm	181 nm
Fill factor	0.49	0.45	0.48	0.46

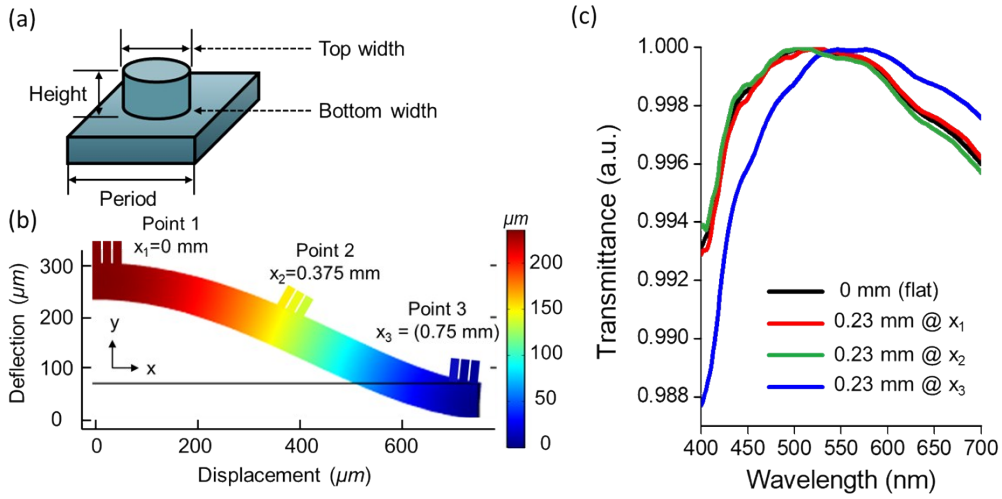

Fig. S7 Variation in transmittance during deformation of a thin PDMS membrane with nanopillars using the FDTD simulation based on the FEA. (a) Geometrical changes of PDMS nanopillars including height, top and bottom width, and period were calculated from the FEA. (b) The initial thickness of PDMS membrane was 72 μm. The deformation of nanopillars located at x_1 = 0 mm, x_2 = 0.375 mm, and x_3 = 0.75 mm for the vertical deformation of 0 mm (default) and 0.23 mm at the center of PDMS membrane. (c) Calculated spectral transmittance at three different positions during the membrane deformation. The variation in transmittance at x_1 and x_2 is negligible regardless of geometrical change, but the variation at x_3 is 0.6 % during the membrane deformation.

Section 5. Switching time (time response) of tunable liquid-filled lens

A switching time of the designed lens from maximum pressure to minimum pressure (0 – 42 kPa) is similar to the typical switching time of liquid-filled lens as mili-seconds region *(N. T. Nguyen et al., "Micro-optofluidic Lenses: A review" 4.3 (2010): 031501)* The actual switching time of the designed lens is shown in **Fig S8**, using pressure regulator (PV 830, WPI Inc.). In case of maximum to minimum pressure (Outflow), the switching time is fast due to the interruption of the hydraulic pressure. On the other hand, the time of minimum to maximum pressure (inflow) may be delayed according to the continuous flow of the hydraulic pressure.

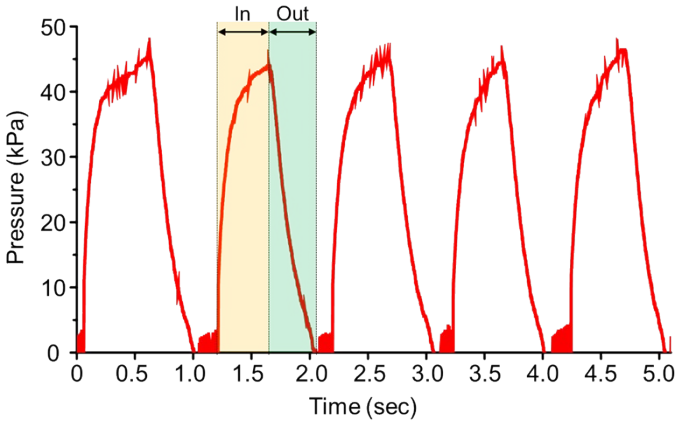

0	Inflow (0 – 42 kPa)	Outflow (42 – 0 kPa)
Average	0.46 sec	0.38 sec
Std	0.049	0.021

Fig S8. Switching time of the designed liquid-filled lens from 0 – 42 kPa pressure range. Switching time in case of pressure outflow (42 kPa to 0 kPa) shows 382 ms, but that of inflow (0 kPa to 42 kPa) shows average time of 464 ms, which may be delayed according to the continuous flow of hydraulic pressure.